

Conversion of electromagnetic and gravitational waves by a charged black hole

Mohamed Ould El Hadj^{✉*} and Sam R. Dolan^{✉†}

Consortium for Fundamental Physics, School of Mathematics and Statistics, University of Sheffield, Hicks Building, Hounsfield Road, Sheffield S3 7RH, United Kingdom

 (Received 28 July 2021; accepted 16 July 2022; published 1 August 2022)

In a strong electromagnetic field, gravitational waves are converted into electromagnetic waves of the same frequency, and vice versa. Here, we calculate scattering and conversion cross sections for a planar wave impinging upon a Reissner-Nordström black hole in electrovacuum, using the partial-wave expansion and numerical methods. We show that, at long wavelengths, the conversion cross section matches that computed by Feynman-diagram techniques, and at short wavelengths, the essential features are captured by a geometric-optics approximation. We demonstrate that the converted flux can exceed the scattered flux at large scattering angles, for highly-charged black holes. In the short-wavelength regime, the conversion effect may be understood in terms of a conversion phase that accumulates along a ray. We compute the scattering angle for which the converted and scattered fluxes are equal, as a function of charge-to-mass ratio; and we show that this scattering angle approaches 90° in the extremal limit.

DOI: [10.1103/PhysRevD.106.044002](https://doi.org/10.1103/PhysRevD.106.044002)

I. INTRODUCTION

The Gertsenshtein-Zel'dovich (GZ) effect [1,2] is the conversion of electromagnetic waves into gravitational waves, and vice versa, in the presence of a strong magnetic field. It is a classical (i.e., nonquantum) phenomenon that is nevertheless extremely weak, since it involves coupling to gravity. In a uniform transverse magnetic field B_\perp , electromagnetic waves (EWs) are converted into gravitational waves (GWs), and vice versa, over a length scale of $L = \frac{\pi}{2} \frac{c}{\sqrt{4\pi\epsilon_0 G B_\perp}} \approx 1.77 \text{ Mpc} \left(\frac{B_\perp}{1 \text{ Gauss}}\right)^{-1}$. The effect is potentially significant in the early Universe [3–5], where the combination of cosmic magnetic fields and primordial gravitational waves could generate distortions of the cosmic microwave background (CMB) spectrum [6].

The interconversion of EWs and GWs in various nonuniform electromagnetic field configurations has been studied from a theoretical perspective. In 1977, De Logi and Mickelson [7] applied Feynman perturbation techniques to study “catalytic” conversion in static electromagnetic fields. The low-energy graviton-to-photon ($g \rightarrow \gamma$) conversion cross section in the Coulomb field of a fixed charge Q in SI units is [7,8]

$$\frac{d\sigma_{g \rightarrow \gamma}}{d\Omega} = \frac{GQ^2}{4\pi\epsilon_0 c^4} \cot^2(\theta/2) (\cos^4(\theta/2) + \sin^4(\theta/2)). \quad (1)$$

*med.ouldelhadj@gmail.com

†s.dolan@sheffield.ac.uk

The first (second) term in parentheses is associated with the cross section for generating an electromagnetic wave of the same (opposite) handedness as the incident gravitational wave [7]. The conversion cross section exhibits a θ^{-2} divergence in the forward direction, distinct in character from the more familiar Rutherford divergence (θ^{-4}). The dominant contribution is from the photon-pole (‘t-pole’) Feynman diagram, rather than the ‘seagull’ diagram of Compton scattering [8].

A macroscopic realization of a fixed charge is the Reissner-Nordström (RN) black hole, of mass M and charge Q . In classical field theory, a RN black hole can support charges of up to $Q_{\text{max}} = M\sqrt{4\pi\epsilon_0 G} \approx 1.7 \times 10^{20} (M/M_\odot) C$. On the other hand, astrophysical black holes are unlikely to possess a charge any greater than 1C per solar mass, some twenty orders of magnitude lower, due to charge-neutralization effects [9].

The conversion of EW and GWs by a RN black hole has been addressed by many authors since 1974 [10–27]. Johnston *et al.* showed that an uncharged massive particle falling into a RN black hole will generate EM waves [10]; and conversely, that an infalling charged particle will generate GWs [12]. Gerlach [14] and Sibgatullin [15] showed that, in the high-frequency (geometric-optics) regime, there is a beating between electromagnetic and gravitational modes, associated with a periodic transfer of energy. Moncrief [17–19] reduced the coupled system of electromagnetic and gravitational perturbation equations on the RN spacetime to a *pair* of decoupled second-order ODEs, for each parity and angular harmonic. Olson and Unruh [16] studied the odd-parity sector in the WKB

regime. Matzner [23] addressed the conversion of an incident planar wave via the partial-wave approach, focusing particularly on the $\ell = 2$ mode. Fabbri [28] also addressed scattering and conversion cross sections. Breuer *et al.* [26] calculated the conversion scattering cross section under the Born approximation. Chandrasekhar [24] extended the work of Moncrief, clarifying the phase relationship between odd and even parity perturbations. Gunter [25] calculated phase shifts, conversion factors and quasi-normal mode frequencies. Torres del Castillo [29,30] derived asymptotic expressions for Maxwell and Weyl scalars from Hertz-Debye potentials. More recently, the $\gamma \rightarrow \gamma$ and $g \rightarrow g$ scattering cross sections were calculated by Crispino *et al.* in Refs. [31,32], and scalar-field scattering was examined in Ref. [33]. The construction of the metric perturbation and vector potential in Regge-Wheeler gauge was described in Refs. [34,35].

In this work, we calculate the scattering and conversion cross sections for a monochromatic planar wave impinging upon a RN black hole, using both the partial-wave method and a geometric-optics approximation. The scattering scenario is described by a pair of dimensionless parameters, $M\omega$ and Q/M . We focus particularly on the differential cross section for the conversion of an incident electromagnetic wave to an outgoing gravitational wave, which is equal to the cross section for the opposite process.

The article is organized as follows. After introducing the linearized Einstein-Maxwell system in Sec. II A, we review the separation of variables method achieved by Moncrief for the RN black hole in Sec. II B. The partial-wave expressions for the scattering amplitudes and cross sections are summarized in Sec. II C. Notes on the numerical method in Sec. II D are followed by a description of the geometric optics approximation in Sec. II E. The key results are presented in Sec. III, and we conclude with a discussion in Sec. IV. Throughout, we adopt units such that $G = c = 4\pi\epsilon_0 = 1$, and ∇_μ denotes the covariant derivative.

II. METHOD

A. The linearized Einstein-Maxwell system

Following the standard approach of Refs. [1,2,10,14,19], we start by assuming that the dynamical variables can be split into the sum of background and perturbation terms, so that the metric and vector potential take the form $g_{\mu\nu} = g_{\mu\nu} + h_{\mu\nu}$ and $A_\mu = A_\mu + \alpha_\mu$, respectively. At linear order, the field equations for the Einstein-Maxwell system ($G_{\mu\nu} = \frac{8\pi G}{c^4} T_{\mu\nu}$ and $\nabla_\nu F^{\mu\nu} = J^\mu$) in electrovacuum are [13,14]

$$\begin{aligned} \square \bar{h}_{\mu\nu} + 2R^\sigma{}_{\mu}{}^\gamma{}_{\nu} \bar{h}_{\sigma\gamma} - 2R_{(\mu}{}^\gamma{}_{\nu)} \bar{h}_{\gamma)} - g_{\mu\nu} R^{\gamma\delta} \bar{h}_{\gamma\delta} + R \bar{h}_{\mu\nu} \\ = -\frac{16\pi G}{c^4} \delta T_{\mu\nu}, \end{aligned} \quad (2a)$$

$$\square \alpha_\mu - R^\nu{}_{\mu} \alpha_\nu = \delta S_\mu. \quad (2b)$$

Here the trace-reversed metric perturbation $\bar{h}_{\mu\nu} = h_{\mu\nu} - \frac{1}{2} h g_{\mu\nu}$ and perturbed vector potential α_μ are in Lorenz gauge: $\nabla^\mu \bar{h}_{\mu\nu} = 0 = \nabla^\mu \alpha_\mu$. Covariant derivatives are taken with respect on the background spacetime, and the d'Alembertian is $\square = g^{\mu\nu} \nabla_\mu \nabla_\nu$. Here $R_{\mu\nu\gamma\sigma}$, $R_{\mu\nu}$, and R denote the Riemann tensor, the Ricci tensor and the Ricci scalar of the background spacetime. The source term δS_μ in the electromagnetic field equation is [14] $\delta S_\mu \equiv 2g^{\nu\gamma} \delta \Gamma^\sigma{}_{\nu[\mu} F_{\gamma]\sigma}$, where $\delta \Gamma^\sigma{}_{\mu\nu} = g^{\sigma\gamma} (\nabla_{(\mu} h_{\nu)\gamma} - \frac{1}{2} \nabla_\gamma h_{\mu\nu})$ is the perturbation in the Christoffel connection due to the metric perturbation, and $F_{\gamma\sigma}$ is the background electromagnetic field tensor. The source term in the gravitational field equation $\delta T_{\mu\nu}$ is given in Refs. [13,14]. In the following sections, we consider the linearized Einstein-Maxwell system for the specific case in which the background spacetime and field tensor correspond to a charged black hole.

B. Perturbations of the Reissner-Nordström spacetime

A RN black hole of mass M and charge Q is described by the line element

$$ds^2 = -f(r)dt^2 + f^{-1}(r)dr^2 + r^2 d\Omega^2, \quad (3)$$

where $f(r) = 1 - 2M/r + Q^2/r^2 = (1 - r_+/r)(1 - r_-/r)$ with $r_\pm = M \pm \sqrt{M^2 - Q^2}$, and $d\Omega^2 = d\theta^2 + \sin^2 \theta d\phi^2$ denotes the line element on the unit 2-sphere S^2 .

Moncrief [17–19] showed that the set of coupled equations governing the metric perturbation and vector potential is amenable to a separation of variables. Assuming harmonic time dependence ($e^{-i\omega t}$), and separating with spin-weighted spherical harmonics, ${}_s Y_\ell^m(\theta)$, the dynamical degrees of freedom are encapsulated by a pair of radial functions $Z_{1\omega\ell}^{(e/o)}(r)$ and $Z_{2\omega\ell}^{(e/o)}(r)$ for each parity (e/o), which are governed by a decoupled pair of second-order ordinary differential equations, viz.,

$$\left\{ \frac{d^2}{dr_*^2} + \omega^2 - V_{s\ell}^{(e/o)}(r) \right\} Z_{s\omega\ell}^{(e/o)}(r) = 0. \quad (4)$$

Here $s \in \{1, 2\}$, and the symbol e (o) denotes even (odd) parity. The tortoise coordinate r_* is defined by $dr_*/dr = 1/f(r)$. Moncrief's odd-parity potential is

$$V_{s\ell}^{(o)}(r) = f(r) \left[\frac{\Lambda + 2}{r^2} - \frac{q_s}{r^3} \left(1 + \frac{6M - q_s}{\Lambda r} \right) \right], \quad (5)$$

where $\Lambda \equiv (\ell - 1)(\ell + 2)$ and

$$q_1 = 3M - \sqrt{9M^2 + 4\Lambda Q^2}, \quad (6a)$$

$$q_2 = 3M + \sqrt{9M^2 + 4\Lambda Q^2}. \quad (6b)$$

(N.B. Here q_1 and q_2 are defined in the opposite order to in Refs. [24,25], in order to simplify the subsequent expressions.)

Chandrasekhar [24,36] showed that Moncrief's even-parity potential can be written as

$$V_{s\ell}^{(e)}(r) = V_{s\ell}^{(o)}(r) + 2q_s \frac{d}{dr_*} \left[\frac{f(r)}{r(q_s + \Lambda r)} \right], \quad (7)$$

and odd and even-parity functions are related by [24,25,36]

$$\begin{aligned} & [\Lambda(\Lambda + 2) \mp 2i\omega q_s] Z_{s\omega\ell}^{(e/o)} \\ &= \left[\Lambda(\Lambda + 2) + \frac{2q_s^2}{r(\Lambda r + q_s)} f(r) \pm 2q_s f(r) \frac{d}{dr} \right] Z_{s\omega\ell}^{(o/e)}. \end{aligned} \quad (8)$$

Here, the upper (lower) sign is associated with the first (second) choice of parity in the superscript.

The relationship between the master variables $Z_{s\omega\ell}^{(e/o)}(r)$ and the metric perturbation and vector potential is summarized in Eqs. (1), (3), and (10) of Ref. [30] (see also Chapter 5 in Ref. [36]).

We now define the modes that are ingoing at the horizon (i.e., in the limit $r \rightarrow r_+$ and $r_* \rightarrow -\infty$) in the standard way,

$$Z_{s\omega\ell}^{\text{in}(e/o)}(r) = \begin{cases} e^{-i\omega r_*}, & r_* \rightarrow -\infty, \\ A_{s\ell\omega}^{(-,e/o)} e^{-i\omega r_*} + A_{s\ell\omega}^{(+,e/o)} e^{+i\omega r_*}, & r_* \rightarrow +\infty, \end{cases} \quad (9)$$

where the coefficients $A_{s\ell\omega}^{(\pm,e/o)}$ are complex amplitudes such that $|A_{s\ell\omega}^{(-,e/o)}|^2 - |A_{s\ell\omega}^{(+,e/o)}|^2 = 1$. It follows from Eq. (8) that the coefficient $A_{s\ell\omega}^{(-,e/o)}$ does not depend on parity

$$A_{s\ell\omega}^{(-,e)} = A_{s\ell\omega}^{(-,o)} \equiv A_{s\ell\omega}^{(-)}, \quad (10)$$

whereas the coefficients $A_{s\ell\omega}^{(+,e/o)}$ are parity dependent,

$$\frac{A_{s\ell\omega}^{(+,e)}}{A_{s\ell\omega}^{(+,o)}} = \frac{\Lambda(\Lambda + 2) + 2i\omega q_s}{\Lambda(\Lambda + 2) - 2i\omega q_s}. \quad (11)$$

The reflection coefficient $\mathcal{R}_s^{(e/o)}$ is

$$\mathcal{R}_s^{(e/o)} \equiv \frac{A_{s\ell\omega}^{(+,e/o)}}{A_{s\ell\omega}^{(-)}}. \quad (12)$$

The electromagnetic (H) and gravitational (Q) perturbations are derived from the radial functions [17–19]

$$H^{(e/o)} \equiv \cos \alpha Z_{1\omega\ell}^{(e/o)} - P \sin \alpha Z_{2\omega\ell}^{(e/o)}, \quad (13a)$$

$$Q^{(e/o)} \equiv P \sin \alpha Z_{1\omega\ell}^{(e/o)} + \cos \alpha Z_{2\omega\ell}^{(e/o)}, \quad (13b)$$

where $P = +1$ for even parity and $P = -1$ for odd parity. Here [17–19],

$$\begin{aligned} \cos^2 \alpha &= \frac{q_2}{q_2 - q_1}, & \sin^2 \alpha &= \frac{-q_1}{q_2 - q_1}, \\ \sin(2\alpha) &= \frac{-2\sqrt{-q_1 q_2}}{q_2 - q_1} = \frac{-2Q\Lambda^{1/2}}{\sqrt{9M^2 + 4\Lambda Q^2}}. \end{aligned} \quad (14)$$

The conversion coefficient $\mathcal{C}^{(e/o)}$ is

$$\mathcal{C}^{(e/o)} = \left| \frac{1}{2} \sin(2\alpha) (\mathcal{R}_1^{(e/o)} - \mathcal{R}_2^{(e/o)}) \right|^2. \quad (15)$$

This is the fraction of the incident wave [in an $\ell\omega$ mode of parity (e/o)] that is converted from electromagnetic to gravitational, and vice versa [36,37].

C. Scattering amplitudes

The amplitudes for planar wave scattering by a RN black hole are summarized below. A full derivation is given in Ref. [38] (see also Refs. [23,39] for details). Here \mathfrak{f} is the helicity-preserving amplitude, and \mathfrak{g} is the helicity-reversing amplitude. The superscripts s_i and s_f refer to the spins of the initial and final fields, with $s = 1$ for an electromagnetic wave and $s = 2$ for a gravitational wave. For example, $\mathfrak{f}^{(11)}$ is the amplitude for scattering a circular-polarized incoming electromagnetic wave to an outgoing electromagnetic wave of the same handedness, and $\mathfrak{g}^{(12)}$ is the amplitude for converting an incoming electromagnetic wave ($s_i = 1$) to an outgoing gravitational wave ($s_f = 2$) of the opposite handedness.

The amplitudes are

$$\begin{aligned} \mathfrak{f}^{(s_i s_f)}(\theta) &= \frac{\pi}{i\omega} \sum_{\ell=\ell_{\min}}^{\infty} [(S_{\ell}^{(e, s_i s_f)} + S_{\ell}^{(o, s_i s_f)}) - 2\delta_{s_i s_f}] \\ &\quad \times {}_{-s_i} Y_{\ell}^{s_i}(0) {}_{-s_f} Y_{\ell}^{s_f}(\theta), \end{aligned} \quad (16a)$$

$$\begin{aligned} \mathfrak{g}^{(s_i s_f)}(\theta) &= \frac{\pi}{i\omega} \sum_{\ell=\ell_{\min}}^{\infty} (-1)^{\ell} [(S_{\ell}^{(e, s_i s_f)} - S_{\ell}^{(o, s_i s_f)})] \\ &\quad \times {}_{-s_i} Y_{\ell}^{s_i}(0) {}_{-s_f} Y_{\ell}^{s_f}(\pi - \theta), \end{aligned} \quad (16b)$$

where $\ell_{\min} \equiv \max(s_i, s_f)$ and $\delta_{s_i s_f}$ is the Kronecker delta. Here ${}_s Y_{\ell}^m(\theta)$ are spin-weighted spherical harmonics. The associated cross section is

$$\frac{d\sigma^{s_i \rightarrow s_f}}{d\Omega} = |\mathfrak{f}^{(s_i s_f)}(\theta)|^2 + |\mathfrak{g}^{(s_i s_f)}(\theta)|^2. \quad (16c)$$

The scattering coefficients in Eqs. (16) are

$$S_\ell^{(e/o,11)} = (-1)^{\ell+1} (\cos^2 \alpha \mathcal{R}_1^{(e/o)} + \sin^2 \alpha \mathcal{R}_2^{(e/o)}), \quad (17a)$$

$$S_\ell^{(e/o,22)} = (-1)^{\ell+1} (\sin^2 \alpha \mathcal{R}_1^{(e/o)} + \cos^2 \alpha \mathcal{R}_2^{(e/o)}), \quad (17b)$$

$$S_\ell^{(e/o,12)} = S_\ell^{(e/o,21)} = (-1)^{\ell+1} \frac{1}{2} \sin(2\alpha) (\mathcal{R}_1^{(e/o)} - \mathcal{R}_2^{(e/o)}), \quad (17c)$$

where $\sin^2 \alpha$, $\cos^2 \alpha$, and $\sin(2\alpha)$ are defined in Eq. (14), and the reflection coefficients in Eq. (12). The square magnitude of the scattering coefficient $S_\ell^{(e/o,12)}$ is equal to the conversion coefficient $\mathcal{C}^{(e/o)}$ of Eq. (15).

In this work, we focus on the conversion cross sections ($s_i \neq s_f$). The $\gamma \rightarrow g$ and $g \rightarrow \gamma$ conversion cross sections are equal, $\frac{d\sigma_{1 \rightarrow 2}}{d\Omega} = \frac{d\sigma_{2 \rightarrow 1}}{d\Omega}$. In the Schwarzschild limit ($Q \rightarrow 0 \Rightarrow \alpha \rightarrow 0$), the conversion cross sections vanish [$\mathbf{f}^{(12)} = \mathbf{g}^{(12)} = 0$]. In this same limit, the helicity-reversing amplitude vanishes in the electromagnetic case [$\mathbf{g}^{(11)} = 0$], but not in the gravitational case [$\mathbf{g}^{(22)} \neq 0$].

D. Numerical method

In order to numerically construct the scattering cross sections (16c), i.e., the scattering amplitudes (16a) and (16b) for the different processes ($\gamma \rightarrow \gamma$, $g \rightarrow g$, and $\gamma \rightarrow g$), we need the scattering coefficients $S_\ell^{(e/o, s_i s_f)}$ (17). For this purpose:

- (1) We have constructed the functions $Z_{s\ell}^{(e/o)}(r)$, the coefficients $A_{s\ell\omega}^{(\pm, e/o)}$ as well as the reflection coefficients $\mathcal{R}_s^{(e/o)}$. To do this, we numerically integrated the second-order ordinary differential equations (4) using the Runge-Kutta method. In order to initialize the process, we start with a Frobenius series expansion of the solution that is regular on the future horizon [Eq. (9)]. We determined the coefficients $A_{s\ell\omega}^{(\pm, e/o)}$ by comparing the numerical solution at large r with the solutions to asymptotic expansions with ingoing and outgoing behavior at spatial infinity. The numerical results were independently performed for the two parities for each spin. To check the robustness and consistency of our numerical calculations, we have used the Chandrasekhar relations (8) and (11).
- (2) We summed 120 ℓ -modes to construct the scattering amplitudes (16a) and (16b) for the different processes. The series representations of the scattering amplitudes in Eqs. (16a) and (16b) suffer of a lack of convergence with ℓ . This is due to the long-range nature of the electromagnetic and gravitational field interactions, or in other words, the $1/r$ falloff in Newtonian/Coulomb potentials, which leads to a divergence of the cross sections in the $\theta \rightarrow 0$ limit. To handle this, we have used the method described

in the Appendix of Ref. [40] to accelerate the convergence of the mode sum. All numerical calculations were performed with the software package *Mathematica*.

E. Rays and the geometric-optics approximation

In the short-wavelength (high-frequency) regime, wave propagation is typically well described by a geometric-optics approximation, in which null geodesics ('rays') play a central role. Introducing the ansatz $\alpha_\mu = \text{Re} \mathcal{A}_\mu e^{i\Phi(x)/\epsilon}$ for the vector potential in Lorenz gauge in vacuum, standard geometric-optics in vacuum (e.g., Box 5.6 in Ref. [41]) yields that (i) the gradient of the phase $k_\mu \equiv \nabla_\mu \Phi$ is tangent to a null geodesic, (ii) the amplitude \mathcal{A} is inversely proportional to the cross-sectional area of ray bundles, and (iii) the polarization vector s_μ is parallel transported along each ray.

Gerlach [14,22] and Sibgatullin [15] have applied the geometric-optics method to address the problem of the conversion of EM and GWs in a background field in the short-wavelength regime, starting with the linearized Einstein-Maxwell equations in Eqs. (2). These authors find that, in an arbitrary electromagnetic field, there are two coupled phenomena: (i) a periodic exchange of energy between electromagnetic and gravitational fields, and (ii) Faraday rotation of the polarization planes. In general, the Faraday rotation necessitates the introduction of Euler angles and a somewhat sophisticated analysis [22]. However, in cases in which the configuration of the ray and the background electromagnetic field is such that the Maxwell scalar ϕ_0 has a constant complex phase along the ray, then phenomenon (ii) is not present [15] and the analysis of (i) is straightforward. This is precisely the case for rays around a Reissner-Nordström black hole, as we now shall describe.

The relevant Maxwell scalar is defined as $\phi_0 \equiv F_{\mu\nu} k^\mu m^\nu$, where $F_{\mu\nu}$ is the background field and m^μ is a transverse, parallel-transported complex null vector satisfying $m \cdot m = m \cdot k = 0$, $m \cdot m^* = 1$ and $k \cdot \nabla m^\mu = 0$ (here $a \cdot b \equiv g_{\mu\nu} a^\mu b^\nu$). As standard, m^μ is constructed from a pair of real transverse unit spacelike vectors, $m^\mu = \frac{1}{\sqrt{2}}(e_1^\mu + ie_2^\mu)$, where $e_1 \cdot e_1 = e_2 \cdot e_2 = 1$, $e_1 \cdot e_2 = 0 = e_i \cdot k$, and $k \cdot \nabla e_i^\mu = 0$ (here $i \in \{1, 2\}$). Now, without loss of generality (due to spherical symmetry), consider a ray in the equatorial plane ($\theta = \pi/2$). We can choose the vector e_2^μ to be the unit, spacelike vector orthogonal to the equatorial plane, $e_2^\mu = [0, 0, (g_{\theta\theta})^{-1/2}, 0]$. This vector is parallel-transported along the ray, that is, it satisfies the preceding conditions. It is quick to see that $F_{\mu\nu} e_2^\nu = 0$ for the RN black hole, since the background field is radial. Consequently ϕ_0 is *real*, and the Faraday rotation phenomenon is absent. The remaining orthogonal vector $e_1^\mu \equiv s^\mu$ lies in the equatorial plane.

A key result in Refs. [14,15] is that, along a ray, the (normalized) EM and GW amplitudes \mathcal{A}_γ and \mathcal{A}_g obey

$$\mathcal{A}_\gamma = \mathcal{A}(\lambda) \sin \chi(\lambda), \quad (18a)$$

$$\mathcal{A}_g = \mathcal{A}(\lambda) \cos \chi(\lambda), \quad (18b)$$

where χ is the *conversion phase*, defined by an integral along the ray,

$$\chi(\lambda) = \sqrt{\frac{G}{c^4}} \int F_{\mu\nu} k^\mu s^\nu d\lambda. \quad (19)$$

For a RN black hole, there is only one nontrivial component of the background field, $F_{tr} = -F_{rt} = Q/r^2$, and so Eq. (19) becomes (with $G = c = 1$)

$$\chi(\lambda) = Q \int \frac{(k^t s^r - k^r s^t)}{r^2} d\lambda. \quad (20)$$

A ray in the equatorial plane has a tangent vector $k^\alpha \equiv dx^\alpha/d\lambda = [E/f, \dot{r}, 0, Eb/r^2]$, where E and b are constants of motion associated with time-translation and axial symmetries of the spacetime. Without loss of generality, we scale the affine parameter λ such that $E = 1$, so that b has the interpretation of an impact parameter of the ray. The null condition $g_{\mu\nu} k^\mu k^\nu = 0$ yields the energy equation, $\dot{r}^2 = 1 - f(r)b^2/r^2 \equiv U(r; b)$. The photon orbit radius r_c (see Fig. 1) and critical impact parameter b_c follow from the conditions $U(r; b) = \partial_r U(r; b) = 0$, yielding

$$r_c = \frac{1}{2}M \left(3 + \sqrt{9 - 8(Q/M)^2} \right), \quad b_c = \frac{r_c}{\sqrt{f(r_c)}}. \quad (21)$$

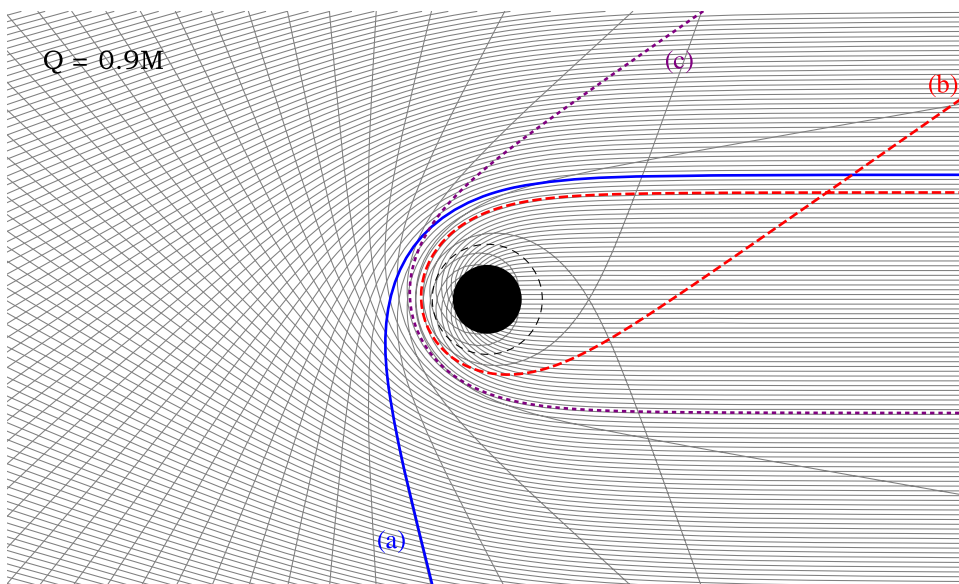


FIG. 1. Parallel rays impinging upon a Reissner-Nordström black hole from the right. In the geometric-optics approximation (high-frequency/short-wavelength limit), the part of the wave incident along ray (a) is half-converted from gravitational waves to electromagnetic waves (or vice versa), and the part of the wave along ray (b) is totally converted. Ray (c) emerges at the same angle as ray (b), generating an interference effect ('orbiting') in the cross sections. The dashed black circle shows the photon orbit.

The orbital equation for a ray with impact parameter b is

$$\left(\frac{du}{d\phi} \right)^2 = \frac{M^2}{b^2} - u^2(1 - 2u + (Q/M)^2 u^2) \equiv \beta(u), \quad (22)$$

where $u \equiv M/r$, and the deflection angle for a ray, Θ , can be expressed formally as an integral,

$$\Theta = 2 \int_0^{u_1} \frac{du}{\sqrt{\beta(u)}} - \pi, \quad (23)$$

where u_1 is the first positive root of the polynomial $\beta(u)$ in Eq. (22).

To determine the conversion phase χ in a similar form, we note that expression (20) is invariant under $s^\mu \rightarrow \tilde{s}^\mu = s^\mu + \kappa(\lambda)k^\mu$, where $\kappa(\lambda)$ is an arbitrary function. Hence it is not necessary to solve the parallel-transport differential equation directly. Instead, we may simply insert a spatial unit spin vector of the form $\tilde{s}_\mu = [0, \tilde{s}_r, 0, \tilde{s}_\phi]$ and impose the algebraic constraints $g^{\mu\nu} \tilde{s}_\mu \tilde{s}_\nu = 1$ and $\tilde{s}_\mu k^\mu = 0$ to determine that $\tilde{s}_r = b/r$. Consequently,

$$\chi = \frac{2Q}{M} \int_0^{u_1} \frac{udu}{\sqrt{\beta(u)}}. \quad (24)$$

In general, Eqs. (23) and (24) may be expressed in terms of elliptic integrals.

In the special case of an extremal black hole, $Q = M$, we find that a certain linear combination of (23) and (24) has an elementary solution, viz.,

$$2\chi - \Theta = \pi + 2 \int_0^{u_1} \frac{(2u-1)du}{\sqrt{\frac{M^2}{b^2} - (u(1-u))^2}} = 0, \quad (25)$$

where $u_1(1-u_1) = M/b$, and the integral is performed with the substitution $v = u(1-u)$. Thus for an extremal black hole ($Q = M$) there is a remarkably straightforward linear relationship between the deflection angle and the conversion phase,

$$\chi = \frac{1}{2}\Theta. \quad (26)$$

The classical scattering cross section is the ratio of the area on the initial wave front of a family of rays, $\delta A = 2\pi b \delta b$, to the solid angle into which they are scattered, $\delta\Omega = 2\pi \sin\theta |d\Theta|$, that is,

$$\left. \frac{d\sigma}{d\Omega} \right|_{cl.} = \frac{b}{\sin\theta |d\Theta/db|}, \quad (27)$$

where $\Theta(b)$ is the deflection function. Implicit in Eq. (27), however, are the assumptions that $\Theta(b)$ is an invertible function (i.e., that there is a single ray associated with a given scattering angle), and that there is no conversion. Below, we seek an extended approximation that remedies both deficiencies.¹

To obtain a (numerical) geometric-optics approximation to the scattering and conversion cross sections, we took the following steps:

- (1) Define a time function $T(b; x_i, r_f)$ (with $x_i, r_f \gg M$ fixed parameters, with $x_i, r_f \sim 1000M$ sufficient for our purposes) corresponding to the coordinate time that it takes for a ray starting on a planar wave front, a perpendicular distance x_i from the origin, to reach to a radius $r = r_f$ after scattering [N.B. $T(b)$ diverges as $b \rightarrow b_c$ and is undefined for $b < b_c$].
- (2) Define the deflection function $\Theta(b; x_i, r_f)$ in a similar way, from the ϕ coordinate at $r = r_f$.
- (3) Solve the parallel-transport equation $k^\mu \nabla_\mu s_\nu = 0$ to calculate the t and r components of the spin vector, starting with initial conditions such that $s_\mu k^\mu = 0$ and $g^{\mu\nu} s_\mu s_\nu = 1$ (relations which are preserved along the ray).
- (4) Calculate the conversion phase $\chi(b; x_i, r_f)$ from the integral along the ray using Eq. (20).
- (5) For a given scattering angle θ , define pseudoamplitudes

¹The classical cross section (27) also fails where the denominator vanishes, i.e., for glories ($\theta = n\pi$) and for rainbows ($\Theta' = 0$). To handle these cases, a more sophisticated semi-classical analysis is required; this is not pursued here.

$$f_{\text{geo}}^{(\text{scat})} = \sum_{k=1}^{\infty} \mathcal{A}_k e^{-i\omega T(b_k)} (-1)^k \cos\chi_k, \quad (28a)$$

$$f_{\text{geo}}^{(\text{conv})} = \sum_{k=1}^{\infty} \mathcal{A}_k e^{-i\omega T(b_k)} \sin\chi_k, \quad (28b)$$

where

$$\mathcal{A}_k = \sqrt{\frac{b_k}{\sin(\theta) |d\Theta_k/db|}}.$$

- (6) The geometric-optics approximations for the scattering and conversion cross sections are given by the square-magnitudes of the amplitudes,

$$\frac{d\sigma^{\gamma \rightarrow \gamma}}{d\Omega_{\text{geo}}} = \frac{d\sigma^{g \rightarrow g}}{d\Omega_{\text{geo}}} = |f_{\text{geo}}^{(\text{scat})}|^2, \quad (29a)$$

$$\frac{d\sigma^{\gamma \rightarrow g}}{d\Omega_{\text{geo}}} = \frac{d\sigma^{g \rightarrow \gamma}}{d\Omega_{\text{geo}}} = |f_{\text{geo}}^{(\text{conv})}|^2. \quad (29b)$$

In principle, the sum in Eq. (28) is taken over *all* rays that emerge at angle θ , in other words, rays with deflection angles $\Theta_1 = \theta, \Theta_2 = 2\pi - \theta, \Theta_3 = 2\pi + \theta, \dots$ and corresponding impact parameters b_1, b_2, b_3 etc. In practice, we sum the contributions from only the primary ($k = 1$) and secondary ($k = 2$) rays, as this is sufficient to reproduce the orbiting oscillation visible in the results.

The divergences in the cross sections in the small-angle limit ($\theta \rightarrow 0$) may be understood in terms of rays in the weak field ($b \gg M$). Using the Einstein deflection angle, $\Theta \sim 4M/b \ll 1$, and the conversion phase for a ray in Minkowski spacetime, $\chi \sim 2Q/b \ll 1$, the scattering and conversion cross sections scale as

$$\frac{d\sigma^{\gamma \rightarrow \gamma}}{d\Omega_{\text{geo}}} = \frac{d\sigma^{g \rightarrow g}}{d\Omega_{\text{geo}}} \sim \frac{16M^2}{\theta^4}, \quad (30a)$$

$$\frac{d\sigma^{\gamma \rightarrow g}}{d\Omega_{\text{geo}}} = \frac{d\sigma^{g \rightarrow \gamma}}{d\Omega_{\text{geo}}} \sim \frac{4Q^2}{\theta^2}, \quad (30b)$$

at small angles.

III. RESULTS

Figure 2 shows helicity-preserving and helicity-reversing conversion cross sections at low frequencies. The cross sections computed via the partial-wave series in Eq. (16) (solid) are compared with the approximation obtained via Feynman-diagram expansions (dashed). More precisely, we compare our numerical results with the cross sections in Eq. (3.19) of De Logi and Mikelson [7],

$$|f_0|^2 = \frac{1}{4} Q^2 \cot^2(\theta/2) (1 + \cos \theta)^2, \quad (31a)$$

$$|g_0|^2 = \frac{1}{4} Q^2 \cot^2(\theta/2) (1 - \cos \theta)^2. \quad (31b)$$

The sum of these terms yields Eq. (1), after restoring dimensionful constants.

In Fig. 2, the comparison is made in the low frequency regime ($2M\omega = 0.1$) for three charge-to-mass ratios: $Q = 0.01 M$, $0.5 M$, and $0.8 M$. In each case, the conversion cross sections are well described by the approximation in Eq. (31). Consistent closed-form results were also obtained via the Born approximation in Ref. [26], and again by Feynman-diagram techniques in Ref. [8].

At higher frequencies, the conversion cross section develops additional structure. Figure 3 shows the conversion cross section at higher frequencies ($2M\omega = 0.1, 1$, and 6) at $Q = 0.5 M$ and $0.8 M$. The dominant contribution is from the helicity-preserving amplitude, and the helicity-reversing amplitude diminishes as $M\omega$ increases. Relatedly, the phase difference between the odd and even parity modes at fixed $(\ell + 1/2)/\omega$, given in Eq. (11), diminishes as ω increases. In other words, a circularly-polarized

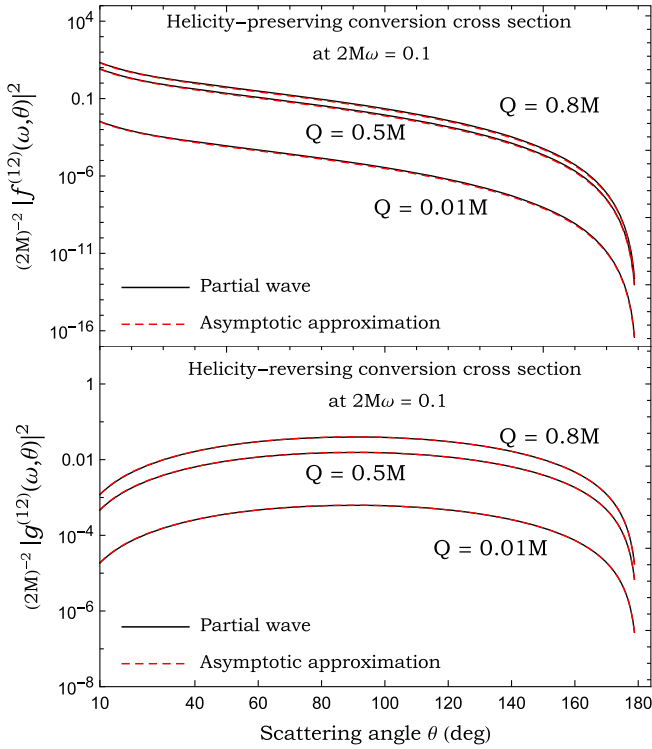


FIG. 2. Comparison of helicity-preserving and helicity-reversing conversion scattering amplitude with asymptotic approximation at low frequency ($2M\omega = 0.1$) for $Q = 0.01 M$, $0.5 M$, and $0.8 M$. The solid line shows the cross section computed from the partial-wave series, Eq. (16), and the dashed line shows the Feynman-expansion result, Eq. (31), of Ref. [7].

incident EW (GW) generates an elliptically-polarized GW (EW) in general, but the elliptical polarization becomes essentially circular at high frequencies.

For $M\omega \gtrsim 1$, Fig. 3 shows regular spiral-scattering (‘orbiting’) oscillations in the cross sections. In the semi-classical interpretation, these are due to the interference between rays scattered by angles $\theta, 2\pi - \theta, 2\pi + \theta, 4\pi - \theta$, etc., [see Fig. 1 and rays (b) and (c)]. The relative phase difference associated with the first and second ray is determined by their path difference; as this increases in a nearly linear fashion with θ , the oscillations are regular. Making the crude, but effective, approximation that the rays circulate on the photon orbit yields an approximate angular width of $\pi/(\omega b_c)$, with b_c given in Eq. (21).

Figure 4 compares the conversion cross section ($\gamma \leftrightarrow g$) with the scattering cross sections ($\gamma \rightarrow \gamma$ and $g \rightarrow g$). At small angles, the conversion cross section exhibits a θ^{-2} divergence in the forward direction, whereas the scattering cross sections exhibit a θ^{-4} divergence, as anticipated in Eq. (30). The conversion cross section is exactly zero in the backward direction $\theta = \pi$, but the scattering cross sections are not zero, due to the nonzero amplitudes $g^{(22)}$ (for $Q \geq 0$) and $g^{(11)}$ (for $Q > 0$ only) [31]. At large angles, regular spiral-scattering oscillations are present for $M\omega \gtrsim 1$. Notably, the conversion cross section can actually exceed the scattering cross section at large scattering angles, as is evident in Fig. 4(d).

Figure 5 shows the scattering and conversion cross sections for a nearly-extremal black hole, with a charge-to-mass ratio $Q/M = 0.99$. At small angles, the scattering cross section ($\sim \theta^{-4}$) dominates over the conversion cross section ($\sim \theta^{-2}$). However, for larger angles $\theta \gtrsim 91^\circ$, the conversion cross section is *larger* than the scattering cross section. In other words, for an incident electromagnetic wave, the energy flux in gravitational waves will exceed that in electromagnetic waves at large angles (and vice versa, for an incident gravitational wave). The three plots show that this effect is rather insensitive to the wave frequency. A satisfying physical explanation for this universality comes from the geometric optics approach devised by Gerlach [14], which associates a conversion factor with each ray (see Fig. 1 and Sec. II E).

Figure 6 compares the geometric-optics approximation (Sec. II E) in Eqs. (28)–(29) (dashed) with the partial-wave cross sections (solid), showing a good qualitative agreement. In the geometric-optics approach, the orbiting oscillations arise from interference between the primary ray, scattered by an angle θ , and the secondary ray, scattered by an angle $2\pi - \theta$ (see Fig. 1). The conversion cross section arises from the accumulated conversion phase χ along a ray. At $\theta \approx 91^\circ$, the conversion phase along the primary ray is $\chi = \pi/4$, implying that half of the energy in the incident wave has been converted [see Eq. (18)]. It is at this angle that, we see the conversion cross section become greater than the scattering cross sections.

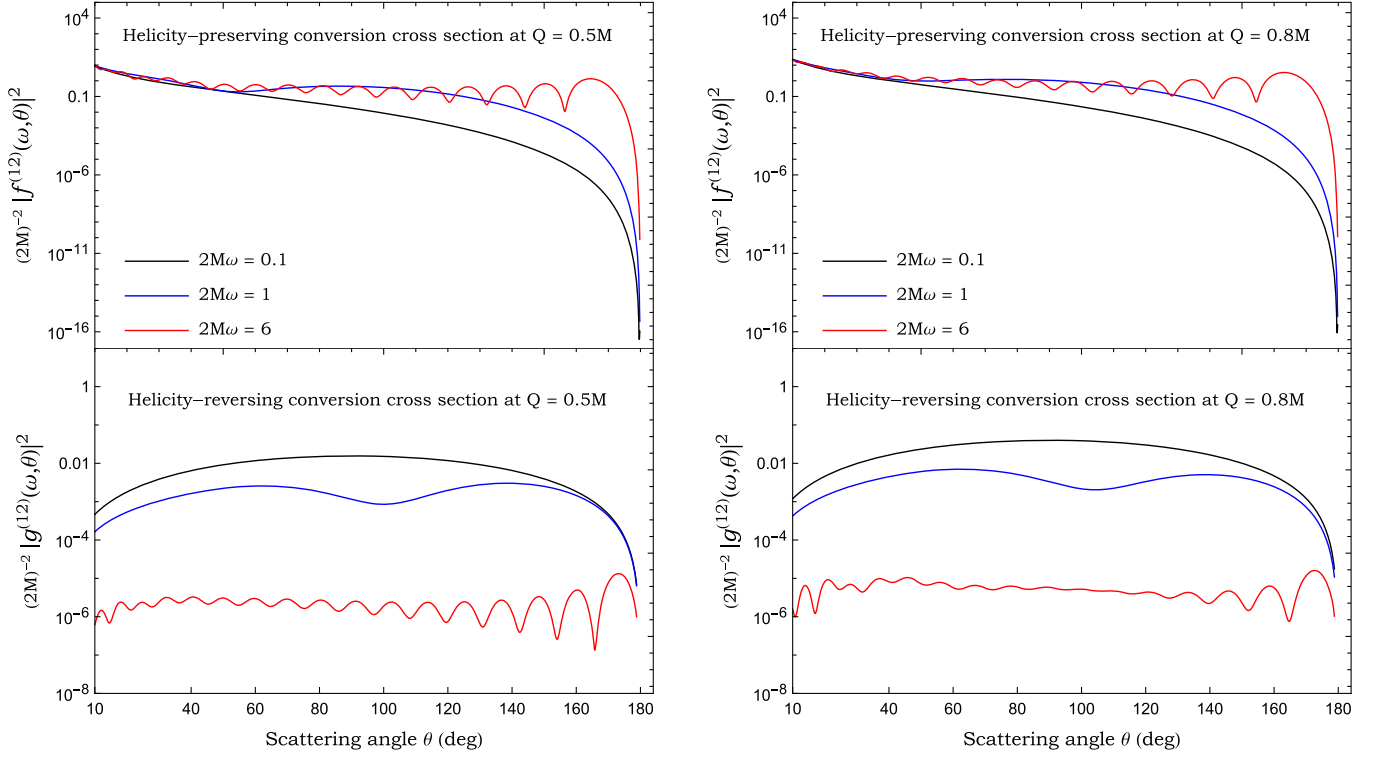


FIG. 3. Helicity-preserving and helicity-reversing conversion cross amplitude for $Q = 0.5 M$ (left panel) and $Q = 0.8 M$ (right panel) at higher frequencies ($2M\omega = 0.1, 1,$ and 6).

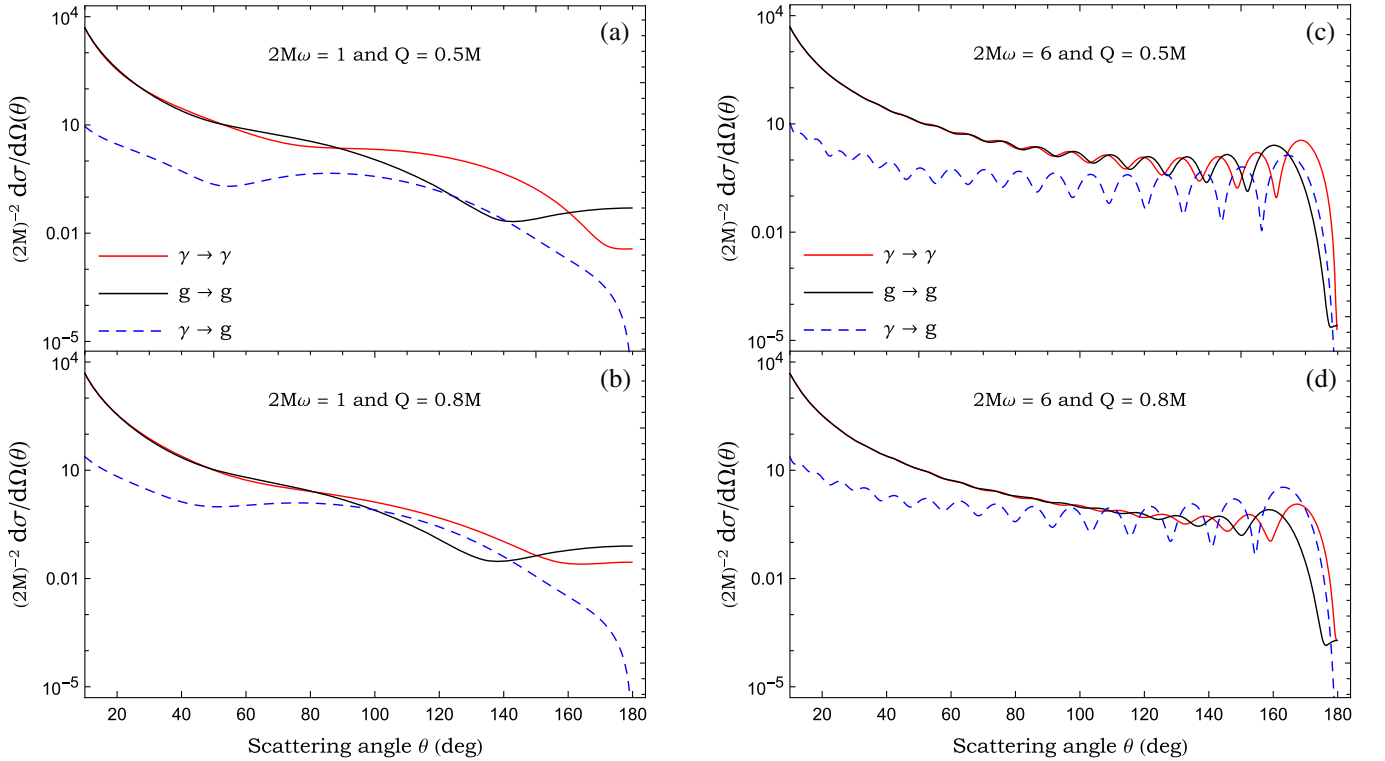


FIG. 4. Scattering and conversion cross sections on the Reissner-Nordström black hole spacetime. The plots compare the scattering cross sections, labeled $\gamma \rightarrow \gamma$ in the electromagnetic-wave case and $g \rightarrow g$ in the gravitational-wave case, with the conversion cross section labeled $\gamma \leftrightarrow g$. The cross section for conversion of an electromagnetic wave to a gravitational wave is equal to the cross section for the conversion of a gravitational wave to an electromagnetic wave. *Left*: Lower frequency $2M\omega = 1$ for (a) $Q = 0.5 M$ and (b) $Q = 0.8 M$. *Right*: Higher frequency $2M\omega = 6$ for (c) $Q = 0.5 M$ and (d) $Q = 0.8 M$.

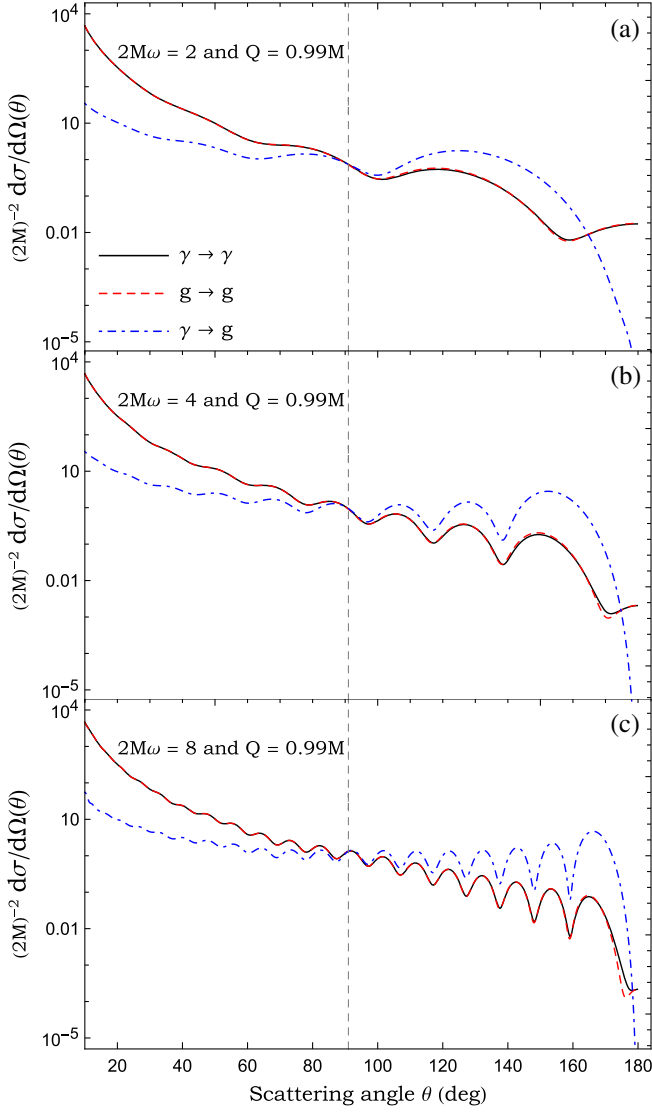


FIG. 5. Scattering and conversion cross sections for a near-extremal Reissner-Nordström black hole ($Q = 0.99M$) at three frequencies: (a) $M\omega = 1$, (b) $M\omega = 2$, and (c) $M\omega = 4$. The $\gamma \rightarrow \gamma$ and $g \rightarrow g$ scattering cross sections (black and red) are almost equal (see Ref. [32]). The $\gamma \leftrightarrow g$ conversion cross section (blue dot-dashed) exceeds the scattering cross section for angles $\theta \gtrsim 91^\circ$.

Having established the validity of the geometric optics approximation (in the regime $M\omega \gg 1$ and away from the poles), we can now compute the scattering angle for which scattering and conversion are equal (in the short-wavelength limit) by examining the conversion phase χ in more detail. This angle was calculated numerically via the method of Sec. II E. Figure 7 shows the angle at which $\chi = \pi/4$ (solid line), as a function of black hole charge, corresponding to half conversion. The line for total conversion ($\chi = \pi/2$) is also shown [dashed].

In the extremal limit $Q = M$, the numerical data supports the simple linear relationship between the conversion phase χ and the deflection angle Θ derived in Eq. (26).

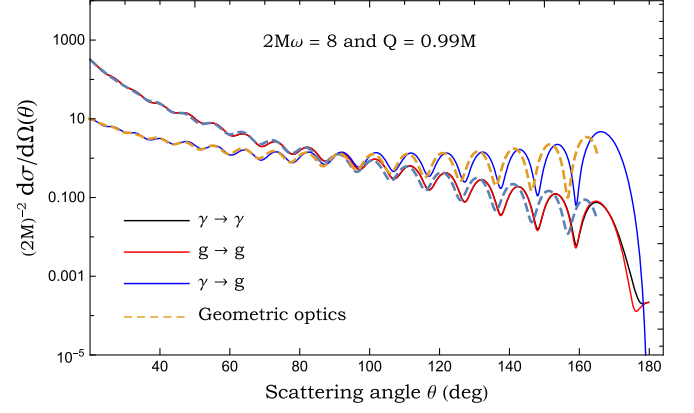


FIG. 6. The geometric-optics approximation. The solid lines show the scattering and conversion cross sections calculated via the partial-wave expansion. The dashed lines show the geometric-optics approximation of Eqs. (28)–(29), obtained by solving transport equations along null rays.

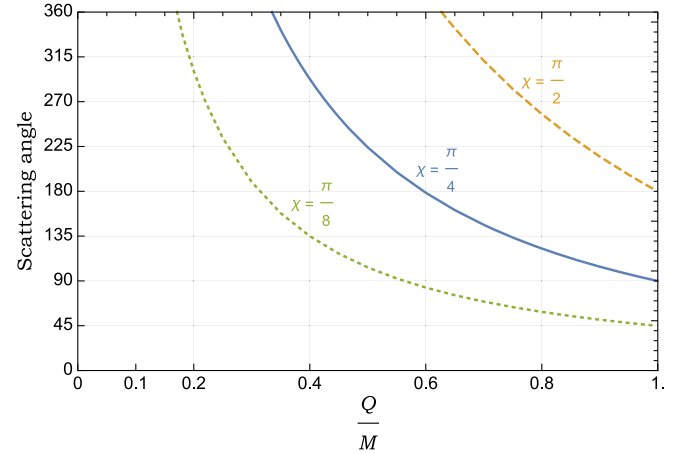


FIG. 7. The scattering angle of the ray corresponding to half conversion ($\chi = \pi/4$) and total conversion ($\chi = \pi/2$) of electromagnetic waves into gravitational waves (and vice versa) in the short-wavelength limit ($M\omega \gg 1$), as a function of charge-to-mass ratio. The curves shown are contours of the conversion phase χ that arises in the geometric-optics approximation (see Sec. II E).

The implication is that, for an extremal black hole, the converted energy will exceed the scattered energy for angles greater than 90° , in the high-frequency regime to which the geometric-optics approximation applies. (A caveat here is that the geometric optics approximation which we have used in Sec. II E breaks down for angles close to $\theta = 180^\circ$, as it is no longer valid to consider pairs of distinct rays, but instead a one-parameter family).

IV. DISCUSSION AND CONCLUSION

In this work, we have calculated the scattering and conversion cross sections for planar electromagnetic and gravitational waves impinging upon a charged black hole.

Accurate numerical results were obtained by summing partial-wave series for the amplitudes, summarized in Sec. II C. In the long-wavelength regime ($M\omega \ll 1$), we found that the conversion cross section matches the Feynman-expansion result [see Eq. (1), Eq. (31), and Fig. 2]. In the short-wavelength regime ($M\omega \gg 1$), the scattering and conversion cross sections are well described by a (numerically-calculated) geometric-optics approximation developed in Sec. II E. This approximation involves calculating Gerlach's conversion phase χ (introduced in Ref. [14]) along the primary and secondary null rays (see Fig. 6).

A key finding of this work is that the converted flux can exceed the scattered flux at large angles, if the black hole is sufficiently charged. In other words, the conversion of electromagnetic waves to gravitational waves with the same frequency—and vice versa—is substantial for parts of the wave front that pass close to the circular photon orbit of a highly-charged black hole. Figure 5 shows this phenomenon for the case $Q = 0.99 M$. In the short-wavelength regime, the (numerical) geometric-optics analysis implies that the converted flux can exceed the scattered flux at large angles if $Q \gtrsim 0.6 M$. The scattering angle beyond which the converted flux exceeds the scattered flux is shown in Fig. 7 (blue solid line); it reaches a minimum of 90° in the extremal case ($Q = M$).

If the incident wave is circular polarized, the outgoing scattered and converted waves are elliptically polarized, in general. At low frequency, the effect is encapsulated by the nonzero helicity-reversing conversion amplitude, g_0 in Eq. (31) [7,8]. In the partial wave expansion, elliptical polarization arises from the difference in phase

shifts between odd- and even-parity perturbations [see Eq. (16b)]. We have demonstrated here that the helicity-reversing amplitudes diminish rapidly as $M\omega$ increases (see Fig. 3), such that in the short-wavelength limit the scattered and converted flux is essentially circular-polarized, with the same handedness as the incident wave.

Here, we have investigated gravitoelectrical conversion in the idealized setting of a charged black hole in vacuum. Astrophysical black holes are not expected to sustain sizable charge-to-mass ratios Q/M [9]. Conversion in the more realistic setting of a black hole magnetosphere coupled to an accretion disk was recently examined in Ref. [42].

An obvious extension of this work is to the *rotating* charged scenario: the Kerr-Newman black hole. The scattering of a scalar field by a Kerr-Newman black hole was studied in [43]. For electromagnetic and gravitational perturbations, a separation of variables has not been achieved, and alternative approaches [44] are necessary to solve the coupled equations in full. On the other hand, the geometric-optics approximation should be straightforward, as the geodesic equations for null rays are (Liouville) integrable.

ACKNOWLEDGMENTS

S. D. thanks Devin Walker, Vitor Cardoso, and Panagiotis Giannadakis for discussions. S. D. acknowledges financial support from the Science and Technology Facilities Council (STFC) under Grant No. ST/T001038/1, and from the European Union's Horizon 2020 research and innovation programme under the H2020-MSCA-RISE-2017 Grant No. FunFiCO-777740.

-
- [1] M. E. Gertsenshtein, Wave resonance of light and gravitational waves, *Sov. Phys. JETP* **14**, 84 (1962).
 - [2] Ya. B. Zel'dovich, Electromagnetic and gravitational waves in a stationary magnetic field, *Zh. Eksp. Teor. Fiz.* **65**, 1311 (1973).
 - [3] Mattias Marklund, Gert Brodin, and Peter K. S. Dunsby, Radio wave emissions due to gravitational radiation, *Astrophys. J.* **536**, 875 (2000).
 - [4] A. D. Dolgov and D. Ejlli, Conversion of relic gravitational waves into photons in cosmological magnetic fields, *J. Cosmol. Astropart. Phys.* **12** (2012) 003.
 - [5] T. Fujita, K. Kamada, and Y. Nakai, Gravitational waves from primordial magnetic fields via photon-graviton conversion, *Phys. Rev. D* **102**, 103501 (2020).
 - [6] V. Domcke and C. Garcia-Cely, Potential of Radio Telescopes as High-Frequency Gravitational Wave Detectors, *Phys. Rev. Lett.* **126**, 021104 (2021).
 - [7] W. K. De Logi and A. R. Mickelson, Electrogravitational conversion cross-sections in static electromagnetic fields, *Phys. Rev. D* **16**, 2915 (1977).
 - [8] N. E. J. Bjerrum-Bohr, B. R. Holstein, L. Planté, and P. Vanhove, Graviton-photon scattering, *Phys. Rev. D* **91**, 064008 (2015).
 - [9] G. W. Gibbons, Vacuum polarization and the spontaneous loss of charge by black holes, *Commun. Math. Phys.* **44**, 245 (1975).
 - [10] M. Johnston, R. Ruffini, and F. Zerilli, Gravitationally Induced Electromagnetic Radiation, *Phys. Rev. Lett.* **31**, 1317 (1973).
 - [11] M. Johnston, R. Ruffini, and M. Peterson, On the solution of the equations governing the coupled emission of gravitational and electromagnetic radiation, *Lett. Nuovo Cimento* **9S2**, 217 (1974).
 - [12] M. Johnston, R. Ruffini, and F. Zerilli, Electromagnetically induced gravitational radiation, *Phys. Lett.* **49B**, 185 (1974).

- [13] F. J. Zerilli, Perturbation analysis for gravitational and electromagnetic radiation in a Reissner-Nordström geometry, *Phys. Rev. D* **9**, 860 (1974).
- [14] U. H. Gerlach, Beat Frequency Oscillations Near Charged Black Holes and Other Electrovacuum Geometries, *Phys. Rev. Lett.* **32**, 1023 (1974).
- [15] N. R. Sibgatullin, Interaction between short gravitational and electromagnetic waves in arbitrary external electromagnetic fields, *Zh. Eksp. Teor. Fiz.* **66**, 1187 (1974).
- [16] D. W. Olson and W. G. Unruh, Conversion of Electromagnetic to Gravitational Radiation by Scattering from a Charged Black Hole, *Phys. Rev. Lett.* **33**, 1116 (1974).
- [17] V. Moncrief, Odd-parity stability of a Reissner-Nordström black hole, *Phys. Rev. D* **9**, 2707 (1974).
- [18] V. Moncrief, Stability of Reissner-Nordström black holes, *Phys. Rev. D* **10**, 1057 (1974).
- [19] V. Moncrief, Gauge-invariant perturbations of Reissner-Nordström black holes, *Phys. Rev. D* **12**, 1526 (1975).
- [20] D. M. Chitre, R. H. Price, and V. D. Sandberg, Electromagnetic radiation due to space-time oscillations, *Phys. Rev. D* **11**, 747 (1975).
- [21] Stephen Boughn, Electromagnetic radiation induced by a gravitational wave, *Phys. Rev. D* **11**, 248 (1975).
- [22] U. H. Gerlach, Faraday rotation near charged black holes and other electrovacuum geometries, *Phys. Rev. D* **11**, 2762 (1975).
- [23] R. A. Matzner, Low frequency limit conversion cross-sections for charged black holes, *Phys. Rev. D* **14**, 3274 (1976).
- [24] S. Chandrasekhar, On the equations governing the perturbations of the Reissner-Nordström black hole, *Proc. R. Soc. A* **365**, 453 (1979).
- [25] D. L. Gunter, A study of the coupled gravitational and electromagnetic perturbations to the Reissner-Nordström black hole: The scattering matrix, energy conversion, and quasi-normal modes, *Phil. Trans. R. Soc. A* **296**, 497 (1980).
- [26] R. A. Breuer, M. Rosenbaum, M. P. Ryan, and R. A. Matzner, Gravitational electromagnetic conversion scattering on fixed charges in the Born approximation, *Phys. Rev. D* **23**, 305 (1981).
- [27] B. Linet, Electrogravitational conversion in the space-time of an infinite straight superconducting cosmic string, *Phys. Lett.* **146A**, 159 (1990).
- [28] R. Fabbri, Electromagnetic and gravitational waves in the background of a Reissner-Nordström black hole, *Il Nuovo Cimento B* (1971–1996) **40**, 311 (1977).
- [29] G. F. Torres de Castillo, Gravitational and electromagnetic perturbations of the Reissner-Nordström solution, *Classical Quantum Gravity* **4**, 1133 (1987).
- [30] G. F. Torres del Castillo and R. Cartas-Fuentevilla, Scattering by a Reissner-Nordström black hole, *Phys. Rev. D* **54**, 4886 (1996).
- [31] L. C. B. Crispino, S. R. Dolan, A. Higuchi, and E. S. de Oliveira, Inferring black hole charge from backscattered electromagnetic radiation, *Phys. Rev. D* **90**, 064027 (2014).
- [32] L. C. B. Crispino, S. R. Dolan, A. Higuchi, and E. S. de Oliveira, Scattering from charged black holes and supergravity, *Phys. Rev. D* **92**, 084056 (2015).
- [33] L. C. B. Crispino, S. R. Dolan, and E. S. Oliveira, Scattering of massless scalar waves by Reissner-Nordström black holes, *Phys. Rev. D* **79**, 064022 (2009).
- [34] R. Zhu and T. Osburn, Inspirals into a charged black hole, *Phys. Rev. D* **97**, 104058 (2018).
- [35] J. Y. J. Burton and T. Osburn, Reissner-Nordström perturbation framework with gravitational wave applications, *Phys. Rev. D* **102**, 104030 (2020).
- [36] S. Chandrasekhar, *The Mathematical Theory of Black Holes* (Oxford University Press, New York, 1985).
- [37] L. C. B. Crispino, A. Higuchi, and E. S. Oliveira, Electromagnetic absorption cross section of Reissner-Nordström black holes revisited, *Phys. Rev. D* **80**, 104026 (2009).
- [38] M. Ould El Hadj and S. R. Dolan (to be published).
- [39] J. A. H. Futterman, F. A. Handler, and R. A. Matzner, *Scattering from Black Holes*, Cambridge Monographs on Mathematical Physics (Cambridge University Press, Cambridge, England, 2012).
- [40] A. Folacci and M. Ould El Hadj, Regge pole description of scattering of scalar and electromagnetic waves by a Schwarzschild black hole, *Phys. Rev. D* **99**, 104079 (2019).
- [41] Eric Poisson and Clifford M Will, *Gravity: Newtonian, Post-Newtonian, Relativistic* (Cambridge University Press, Cambridge, England, 2014).
- [42] K. Saito, J. Soda, and H. Yoshino, Universal 10^{20} Hz stochastic gravitational waves from photon spheres of black holes, *Phys. Rev. D* **104**, 063040 (2021).
- [43] L. C. S. Leite, C. L. Benone, and L. C. B. Crispino, On-axis scattering of scalar fields by charged rotating black holes, *Phys. Lett. B* **795**, 496 (2019).
- [44] P. Pani, E. Berti, and L. Gualtieri, Gravitoelectromagnetic Perturbations of Kerr-Newman Black Holes: Stability and Isospectrality in the Slow-Rotation Limit, *Phys. Rev. Lett.* **110**, 241103 (2013).